Catalysis Today 175 (2011) 183–188

Contents lists available at ScienceDirect

Catalysis Today

journal homepage: www.elsevier.com/locate/cattod

Selective catalytic oxidation of H_2S over V_2O_5-supported Fe-pillared montmorillonite clay

Kanattukara Vijayan Bineesh [a], Moon-IL Kim [a], Moon-Seok Park [a], Kwan-Young Lee [b], Dae-Won Park [a,*]

[a] School of Chemical and Biomolecular Engineering, Pusan National University, Jangjeon-dong, Gumjeong-gu, Busan 609-735, Republic of Korea
[b] Department of Chemical and Biological Engineering, Korea University, Seoul, 136-701, Republic of Korea

ARTICLE INFO

Article history:
Received 6 October 2010
Received in revised form 7 February 2011
Accepted 14 March 2011
Available online 13 April 2011

Keywords:
Selective catalytic oxidation
Hydrogen sulfide
Sulfur
Pillared clay
Vanadia

ABSTRACT

The selective catalytic oxidation of hydrogen sulfide to elemental sulfur in a continuous-flow fixed-bed reactor was studied over V_2O_5-supported Fe-pillared clay (V/Fe-PILC) catalysts. The synthesized catalysts were characterized by X-ray diffraction (XRD), surface area–pore volume measurements, chemical analysis, X-ray photoelectron spectroscopy (XPS), temperature-programmed desorption of ammonia (NH_3-TPD), and thermogravimetric (TG) analysis. The reaction tests were conducted at temperatures ranging from 220 to 300 °C. The V/Fe-PILC catalysts exhibited very good catalytic performance toward H_2S oxidation at 220–300 °C without much SO_2 emission. The H_2S conversion over V/Fe-PILC increased with increasing vanadia content up to 7 wt.%. This superior catalytic performance might be related to the uniform dispersion of vanadia species on the Fe-PILC support.

1. Introduction

Hydrogen sulfide (H_2S) is one of the most common gases accompanying fuels in oil and gas refinery processes. The sulfur content in gasoline and diesel fuel reduces the fuel quality, resulting in the emission of sulfur dioxide exhaust from engines. These emissions contribute to sore throats, breathing difficulties, respiratory infections, acid rain, and dirty-looking air. Moreover, sulfur compounds in gasoline deactivate the catalytic converters in vehicles and combustion equipments. International environmental regulations concerning the release of sulfur-containing gases have become more stringent, and the H_2S contained in acidic gases now must be carefully controlled before emission to the atmosphere. The demand for a cleaner environment and high-quality fuel has triggered studies on the synthesis of novel, and more efficient catalysts for the removal of H_2S. For many years, most H_2S in petroleum refineries and natural gas plants has been removed using the well-known Claus process [1]. However, because of thermodynamic limitations, 3–5% of the H_2S is not converted to sulfur.

Various commercial processes based on adsorption, absorption, and wet oxidation have been used to treat tail gases containing low concentrations (<5 vol.%) of sulfur-containing gases from Claus plants or other emission sources [2–4]. The most attractive of these is dry catalytic oxidation of H_2S to elemental sulfur after hydrogenation of the sulfur-containing gas to H_2S. Two important commercially developed processes are the Mobil direct oxidation process (MODOP) [1,5] and the Super Claus process [1,6]. They are based on the irreversible selective oxidation of H_2S to sulfur [reaction (1)] as the main reaction, with other oxidation reactions [reactions (2) and (3)] and the reversible Claus reaction (reaction (4) as side reactions).

$$H_2S + 1/2O_2 \rightarrow 1/nS_n + H_2O \quad (1)$$

$$1/nS_n + O_2 \rightarrow SO_2 \quad (2)$$

$$H_2S + 3/2O_2 \rightarrow SO_2 + H_2O \quad (3)$$

$$2H_2S + SO_2 \leftrightarrow 3/nS_n + 2H_2O \quad (4)$$

Clay materials have long been used for catalysis, adsorption and ion-exchange, but their efficient use is limited by their lack of porosity and low thermal stability [7,8]. The oil embargo in 1973 stimulated the investigation and development of modified forms of clays called pillared layered clays (PILCs) [9]. PILCs are obtained by exchanging the charge-compensating cations between clay layers for large inorganic cations followed by calcination. On heating, the intercalated cations are converted to metal oxide clusters, which act as pillars to prop open the layers and generate interlayer spaces of molecular dimensions [10–14]. The physico-chemical properties of PILCs may change depending on the pillar species used. Thus, pillared derivatives of clays have received widespread interest as a new type of layered material that can serve as shape-selective catalysts, separating agents, supports, and sorbents etc. A number of

* Corresponding author. Tel.: +82 51 510 2399; fax: +82 51 512 8563.
E-mail address: dwpark@pusan.ac.kr (D.-W. Park).

0920-5861/$ – see front matter © 2011 Published by Elsevier B.V.
doi:10.1016/j.cattod.2011.03.033

authors have published many works related to iron-oxide-pillared clays [15–24]. Several studies have also reported the selective catalytic oxidation of H_2S or the removal of H_2S using a variety of catalysts [25–35]. In our previous work [36,37], we reported the catalytic performance of vanadia-supported zirconia-pillared clay for the selective catalytic oxidation of H_2S. In the present work, we studied the catalytic performance of Fe-pillared clay and vanadia-loaded Fe-pillared clay for the selective catalytic oxidation of H_2S. We also studied the acidic properties and thermal stabilities of the prepared catalysts.

2. Experimental

2.1. Catalyst synthesis

The starting material was Na-montmorillonite (Kunipia-F, Kunimine Industrial Company) with a cation exchange capacity of 120 mequiv./100 g, which is referred to as Na-MMT. $FeCl_3{\cdot}6H_2O$ (97%, Aldrich) was used to prepare polymeric hydroxy-iron (III) cations. The pillaring solution was obtained by slowly adding a 0.4 M NaOH solution to a 0.2 M $FeCl_3$ solution with constant stirring to obtain the required OH/Fe molar ratio of 2. The mixture was aged for 6 h with stirring at room temperature. The pillaring processes were performed with 2 wt.% clay slurry. The pillaring solutions were then added dropwise to the aqueous clay suspension at 40 °C with stirring to obtain a final Fe/clay ratio of 60 mmol/g. The slurry was kept under stirring for 24 h at room temperature. After aging for 12 h, the product was filtered, washed several times with distilled water, dried in air, and then calcined at 400 °C for 3 h. The final product is referred to as Fe-PILC.

Vanadia-loaded Fe-PILC samples containing 2, 4, 7, and 10 wt.% vanadia were prepared by wet impregnation of the Fe-PILC support with a solution of NH_4VO_3 (99%, Aldrich) dissolved in water acidified by oxalic acid. Finally, all the samples were dried at 80 °C for 20 h and calcined at 400 °C for 3 h under an air flow. The samples were labeled as *x* wt.% V/Fe-PILC, where *x* refers to the vanadia loading on the support.

2.2. Characterization of the catalysts

The chemical composition of the samples was determined by X-ray fluorescence spectroscopy (XRF, Philips PW 2400).

The X-ray diffraction (XRD) patterns were obtained on a Bruker Advanced D8 powder diffractometer, using Ni-filtered Cu Kα radiation (λ = 1.5404 Å). A fixed power source (40 kV, 300 mA) and a scan speed of 0.02° $2\theta\,min^{-1}$ were applied to determine the XRD patterns.

The surface areas were determined by N_2 adsorption at 77 K using a Micromeritics ASAP 2010 instrument. The samples were outgassed in vacuum for 12 h at 110 °C before nitrogen adsorption. The specific surface areas were calculated using the BET equation. The total pore volumes were evaluated from the nitrogen uptake at a relative N_2 pressure of $P/P_0 = 0.99$.

X-ray photoelectron spectroscopy (XPS) analyses were performed using an X-ray photoelectron spectrometer (VG, ESCALAB 250) with monochromatic Al Kα radiation ($h\upsilon$ = 1486.6 eV). Samples calcined at 400 °C for 3 h were pressed into self-supporting wafers without a binder, followed by pretreatment in an ultrahigh vacuum. The binding energies (BE) were calculated using the C 1s band (284.6 eV) as a reference.

To determine the acidity of the catalysts, temperature-programmed desorption of ammonia (NH_3-TPD) was performed with a BEL-CAT chemisorption apparatus (BEL, Japan). Accurately 50 mg of a sample was reheated at 400 °C for 2 h under a He flow and cooled to ambient temperature. Pure ammonia gas (50 $cm^3\,min^{-1}$) was adsorbed at 100 °C for 20 min. After NH_3 was swept with He, the temperature was increased up to 700 °C at a heating rate of 10 °C min^{-1}.

Thermogravimetric (TG) analyses were performed on 10 mg of each sample with a Perkin Elmer TGA 7 apparatus under a nitrogen flow of 50 ml min^{-1} using a heating rate of 20 °C min^{-1} from room temperature to 800 °C.

2.3. Reaction tests

Reaction tests were conducted in a continuous-flow fixed-bed reactor made from a Pyrex tube with a 1-in. internal diameter. The gas flow rate was controlled using mass flow controllers (Brooks MFC, 5850E). A mixture of gases, H_2S, O_2 and a balance of He with purity of 50%, 98%, 99.999%, respectively were used. A sulfur condenser was attached at the effluent side of the reactor, and its temperature was maintained at 110 °C to allow the condensation of sulfur vapor only. A line filter was installed after the condenser to trap any sulfur mist that not captured by the condenser. From the condenser to the gas chromatograph, all lines and fittings were heated to more than 120 °C to prevent condensation of water vapor. In a typical experiment, the reactant composition consisted of 5 vol.% H_2S, 2.5 vol.% O_2, and the balance He. The gas hourly space velocity (GHSV) was fixed at 10,000 h^{-1}. Typically, 0.4 g of catalyst was used with a total gas flow rate of 100 ml min^{-1}.

The O_2, H_2S, and SO_2 contents of the effluent gas were analyzed by a gas chromatograph (HP 5890) equipped with a thermal conductivity detector and a 1.8-m Porapak T column (80–100 mesh) at 100 °C. The exit gas from the analyzer was passed through a trap containing a concentrated NaOH solution and vented out to a hood.

3. Results and discussion

3.1. Chemical composition

The chemical compositions of the initial clay, Fe-PILC, and V/Fe-PILCs obtained by XRF are presented in Table 1. The pillaring of the initial clay by Fe_2O_3, with complete replacement of the interlayer Na cations, increased the Fe_2O_3 content. This increase in Fe_2O_3 content, with a corresponding decrease in the amount of exchangeable Na cations, points to successive replacement of interlayer cations with stable Fe_2O_3 species. The relative amounts of silica, aluminum and magnesium remained almost constant in all samples after pillaring. This suggests that the composition of the clay sheet is preserved in Fe-PILC and the V/Fe-PILCs. A slight decrease in the Fe_2O_3 content was observed after Fe-PILC was impregnated with vanadia.

3.2. Textural and structural properties

Table 2 shows the textural data obtained by BET surface area analysis. The BET surface area of Fe-PILC was 206 m^2/g, whereas that of the initial clay was only 26 m^2/g. The large increase in the surface area of Fe-PILC indicates successful pillaring of Fe_2O_3 species into the silicate layers of the clay [38]. During the pillaring process, the expansion in the clay structure contributed greatly to the enhancement of the surface area and porosity of the clay materials [37,39]. The high surface area obtained by pillaring allows good vanadia dispersion on Fe-PILC. However, an increase in the vanadia loading on the Fe-PILC support decreased the surface area and total pore volume, which might be caused by pore blockage due to progressive filling with vanadia species [37,40,41].

Fig. 1 shows the low-angle XRD patterns of the Na-MMT and Fe-PILC calcined at 400 °C. Na-MMT shows a main peak at a 2θ value of approximately 7°, which is commonly assigned to the basal (0 0 1) reflection (d(0 0 1)). In Fe-PILC, the d(0 0 1) peak was found to shift

Table 1
BET surface area (S_{BET}), total pore volume (V_p) and chemical composition (wt.%) of the samples investigated.

Samples	S_{BET} (m^2/g)	V_p (cm^3/g)	SiO_2	Al_2O_3	Fe_2O_3	Na_2O	V_2O_5
Na-MMT	26	–	56.68	29.20	2.24	4.51	–
Fe-PILC	206	0.256	40.98	24.69	30.13	≪	–
2 wt.% V/Fe-PILC	178	0.213	40.35	23.70	27.91	≪	2.05
4 wt.% V/Fe-PILC	163	0.184	40.31	23.40	24.11	≪	4.45
7 wt.% V/Fe-PILC	152	0.177	40.52	24.48	18.70	≪	7.48
10 wt.% V/Fe-PILC	136	0.169	39.21	24.53	17.10	≪	10.39

≪: less than 0.001 wt.%.

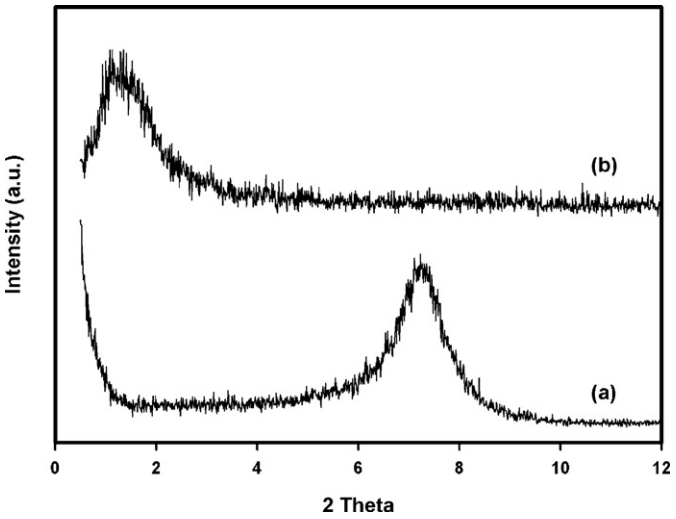

Fig. 1. Low-angle X-ray diffraction patterns: (a) Na-MMT and (b) Fe-PILC.

toward a lower 2θ value, indicating expansion in the layer structure as a result of pillaring [20,38,42]. A diffraction peak representing the (0 0 1) reflection of Na-MMT was found to be totally absent in the pillared clay samples. This proves that iron-oxide pillars are well distributed in the clay and there were no contributions from an unpillared portion to the product obtained. Large and hydrated Fe polyoxocations introduced into the interlayer spaces of the clay push the sheets apart, increasing the d-spacing. Calcination of Fe-intercalated clays leads to dehydration and dehydroxylation of Fe polycations and gives rise to the formation of polymeric Fe_2O_3 species, which permanently link adjacent layers [38]. The d-spacing of Fe-PILC calcined at 400 °C was found to be 63 Å.

3.3. X-ray photoelectron spectroscopy

XPS is one of the most frequently used techniques in catalysis: it provides information about the catalyst surface. This is useful, as the ratio of vanadium oxide to support oxide provides information on the dispersion of the vanadium oxide phase on the support. The surface oxidation states and binding energies (BE) of vanadium and iron were also analyzed by XPS. Table 2 shows the binding energies of Fe $2p_{3/2}$ and V $2p_{3/2}$. The BE of Fe $2p_{3/2}$ was observed at 710 eV, which corresponds to Fe in the +3 oxidation state in Fe-PILC.

Table 2
XPS analysis data of the samples.

Catalysts	Binding energy (eV)	
	Fe $2p_{3/2}$	V $2p_{3/2}$
Fe-PILC	710.2	–
2 wt.% V/Fe-PILC	710.1	517.2
4 wt.% V/Fe-PILC	710.0	517.1
7 wt.% V/Fe-PILC	710.2	517.0
10 wt.% V/Fe-PILC	710.2	517.2

A binding energy of around 517 eV, corresponding to V $2p_{3/2}$, was observed for all the V/Fe-PILC catalysts. This indicates that most of the vanadium occurs mainly in the +5 valence form on the Fe-PILC support [36,37,41,43,44].

Fig. 2 shows a plot of the XPS surface atomic ratios $(V/Fe)_s$ vs. the corresponding bulk ratios $(V/Fe)_b$. An almost linear increase in surface atomic ratio was observed as the loading increased from 2 to 7 wt.%, showing a uniform dispersion of vanadium on Fe-PILC up to 7 wt.%. For 10 wt.% of vanadia, an increase in surface atomic ratio was observed, but it was lower than that from 2 to 7 wt.%. This behavior confirms that at 10 wt.% of vanadia, multilayer patches of bulk-like vanadium oxide particles form [36,37,41], decreasing the dispersion of vanadia on the Fe-PILC support.

3.4. Temperature-programmed desorption of ammonia (NH_3-TPD)

Fig. 3 shows the NH_3-TPD profiles of the Fe-PILC and the V/Fe-PILCs. The pillared clays generally contain both Brönsted and Lewis acid sites [37,40,45]. These acid sites arise from the exposure of the clay structure and the pillar metal oxide [37,40,45,46]. The acid sites in Fe-PILC could be classified into weak (desorption at 150 °C) and strong (desorption at 600 °C) acid sites. The peak at low temperature is due to ammonia desorption from the weak Brönsted acid sites, whereas that at high temperature corresponds to the desorbed ammonia from the strong Lewis acid sites. These Lewis and Brönsted acid sites present on the Fe-PILC arise from the iron-oxide pillars and the structural hydroxyl groups of the montmorillonite layer, respectively. Thus, the Fe-PILC data demonstrated the presence of both Lewis and Brönsted acidities, with Lewis acidity being dominant.

The desorption pattern shows that the addition of vanadia onto Fe-PILC induces an increase in the intensity of the first peak (150 °C) due to the Brönsted acid sites. This demonstrates a change in the

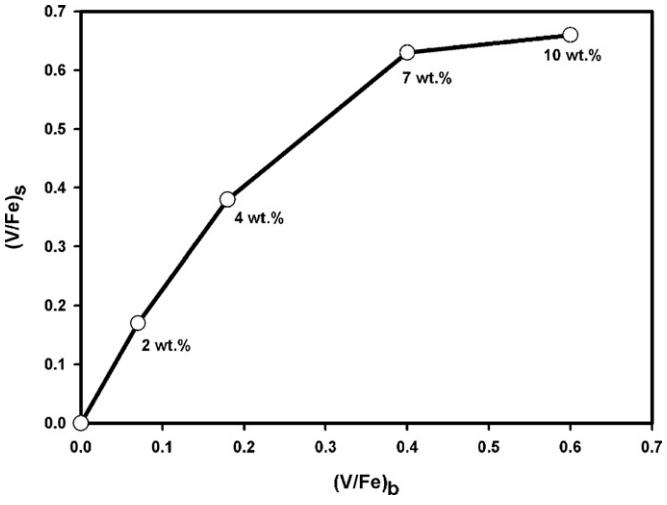

Fig. 2. XPS (V/Fe) surface atomic ratio vs. the corresponding (V/Fe) bulk ratio.

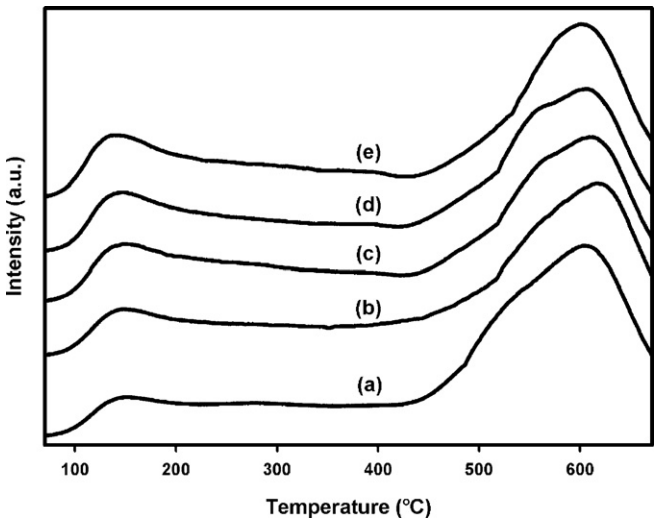

Fig. 3. NH_3-TPD profiles: (a) Fe-PILC, (b) 2 wt.% V/Fe-PILC, (c) 4 wt.% V/Fe-PILC, (d) 7 wt.% V/Fe-PILC and (e) 10 wt.% V/Fe-PILC.

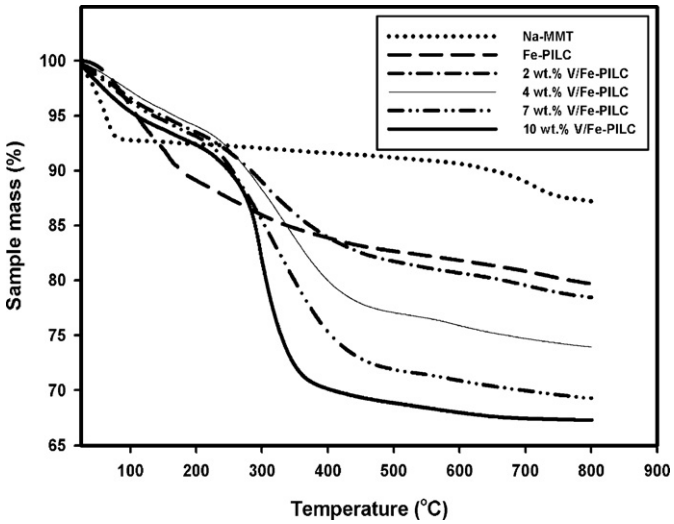

Fig. 4. Thermogravimetic analysis curves of the samples.

surface acidic properties of Fe-PILC with the introduction of vanadia. Thus, the addition of vanadia improves the Brönsted acidity for all V/Fe-PILC catalysts. Similar results have already been observed on vanadia-supported pillared clay catalysts [37,40].

The total amount of ammonia desorbed decreases continuously with increasing vanadia content. Though the addition of vanadia increases the Brönsted acidity, the total acidity diminishes slightly, leading us to conclude that the deposition of vanadia obstructs some pores of the support and reduces the density of strong Lewis acid sites arising from the pillar species [18].

3.5. Thermogravimetric (TG) analyses

The TGA curves of the samples are shown in Fig. 4. For Na-MMT, the weight loss observed at 25–150 °C is due to the removal of physically adsorbed water molecules. Between 150 and 500 °C, a very small weight loss was observed, which is attributed to the removal of interlayer water and the onset of dehydroxylation. Finally, dehydroxylation of the clay structure occurs between 500 and 800 °C, with an inflection point around 700 °C due to the collapse of the clay structure [36,41,47]. For Fe-PILC, the total weight loss was greater, but less pronounced, than that of the original clay. Fe-PILC showed a monotonous weight loss up to 800 °C due to dehydration and dehydroxylation of the pillars and dehydroxylation of the clay structure, without any well-defined inflection point at high temperature. Similar thermal behaviors have been reported previously for Ti-PILC and Zr-PILC catalysts [45]. After the addition of vanadia onto Fe-PILC, a new weight loss appeared around 300 °C, which can be attributed to the dehydroxylation of vanadia species. The TG patterns for all vanadia-loaded samples were qualitatively similar, but the weight loss around 300 °C increases with increasing vanadia wt.% on Fe-PILC. Recently, Bineesh et al. [36] and Arfaoui et al. [48] reported similar weight loss trends in vanadia-loaded pillared clay catalysts prepared by impregnation techniques.

Table 3
Selectivity to SO_2 and S at different temperatures.

Catalyst	Temp. (°C)	S–SO_2 (%)	S–S (%)
2 wt.% V/Fe-PILC	220	3.2	96.8
	240	3.4	96.6
	260	3.8	96.2
	280	4.9	95.1
	300	3.7	96.3
4 wt.% V/Fe-PILC	220	3.0	97.0
	240	4.1	95.9
	260	3.3	96.7
	280	3.9	96.1
	300	4.5	95.5
7 wt.% V/Fe-PILC	220	3.7	96.3
	240	3.3	96.7
	260	3.6	96.4
	280	4.4	95.6
	300	4.2	95.8
10 wt.% V/Fe-PILC	220	3.6	96.4
	240	4.0	96.0
	260	3.8	96.2
	280	4.8	95.2
	300	4.7	95.3

Reaction condition: $H_2S/O_2/He = 5/2.5/92.5$, GHSV = 10,000 h^{-1}, reaction time = 2 h.

3.6. Catalytic performance

Fig. 5 shows the catalytic performance of the V/Fe-PILC catalysts for H_2S oxidation with a reactant composition of $H_2S/O_2/He = 5/2.5/92.5$ at GHSV = 10,000 h^{-1}. For all the V/Fe-PILC

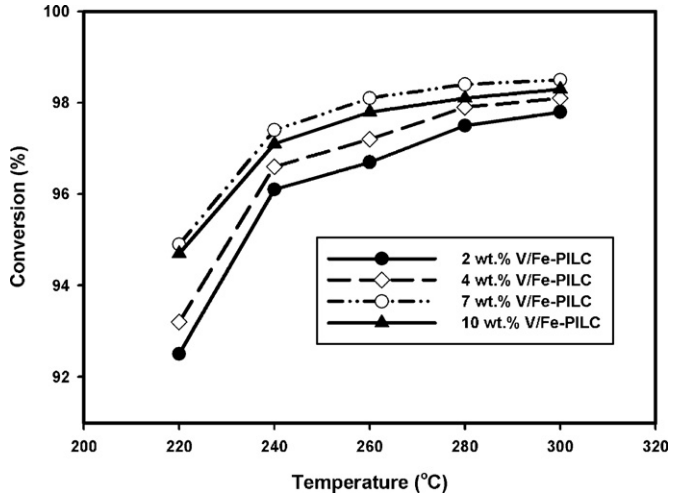

Fig. 5. Conversion of H_2S with V/Fe-PILC catalysts at different temperatures (reactant composition in vol.%: $H_2S/O_2/He = 5/2.5/92.5$, GHSV = 10,000 h^{-1}).

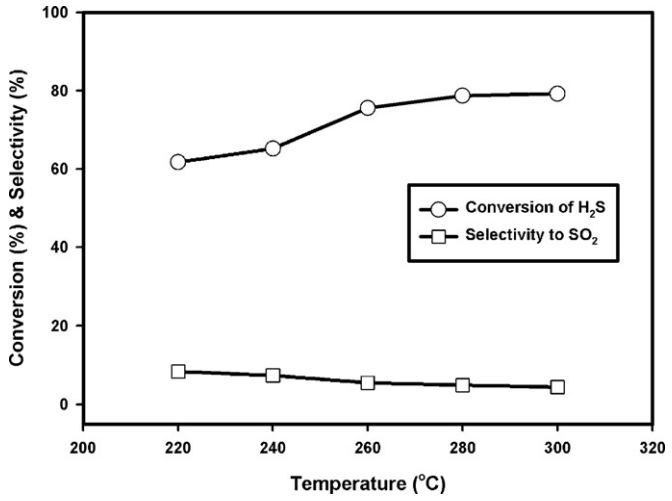

Fig. 6. Conversion of H_2S and selectivity to SO_2 for the support Fe-PILC at different temperatures (reactant composition in vol.%: $H_2S/O_2/He = 5/2.5/92.5$, GHSV = 10,000 h^{-1}).

catalysts, the H_2S conversion increased with increasing temperature. This trend is similar to that previously observed with supported vanadia catalysts [32,36,37,40]. Most of the H_2S was converted to elemental sulfur through selective catalytic oxidation. The addition of vanadia to Fe-PILC increased the catalytic performance. The activity of the vanadia-supported catalysts depends on the nature of the surface vanadia species present in the catalyst. An increase in H_2S conversion was observed when the vanadia loading increased from 2 wt.% to 7 wt.%. This may be due to good dispersion of vanadia species on the Fe-PILC support [36,37,43]. This result agrees well with the XPS data for the samples, which showed a uniform dispersion of vanadium on the surface of Fe-PILC up to a vanadia content of 7 wt.%.

A decrease in H_2S conversion was observed at a vanadia loading of 10 wt.%. This might be due to the formation of a comparatively less reactive aggregated form of vanadia, which decreases the uniform dispersion of vanadia on the support [36,37,40,43]. The decrease in catalytic performance at higher loadings can also be explained by the decrease in specific surface area and pore volume caused by pore blockage by the vanadia species.

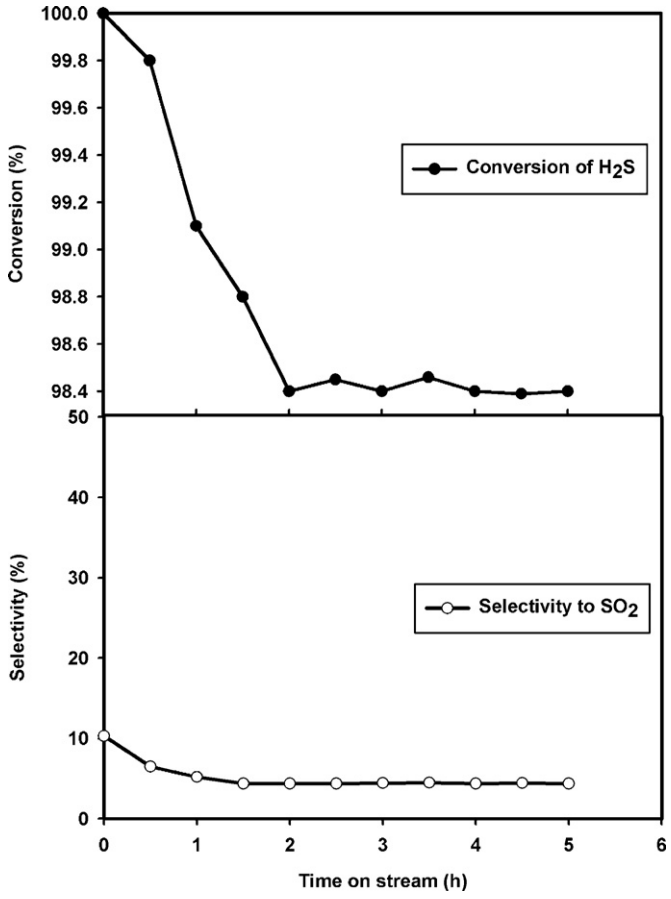

Fig. 7. Time variant conversion of H_2S and selectivity to SO_2 for 7 wt.% V/Fe-PILC at 280 °C (reactant composition in vol.%: $H_2S/O_2/He = 5/2.5/92.5$, GHSV = 10,000 h^{-1}).

Table 3 shows the selectivity for elemental sulfur at temperatures of 220–300 °C for all V/Fe-PILC catalysts. Interestingly, the selectivity remained almost constant at 95–97% for all V/Fe-PILC catalysts, even though the conversion varied over a wide range. This suggests that the sulfur selectivity of these catalysts is less sensitive to temperature.

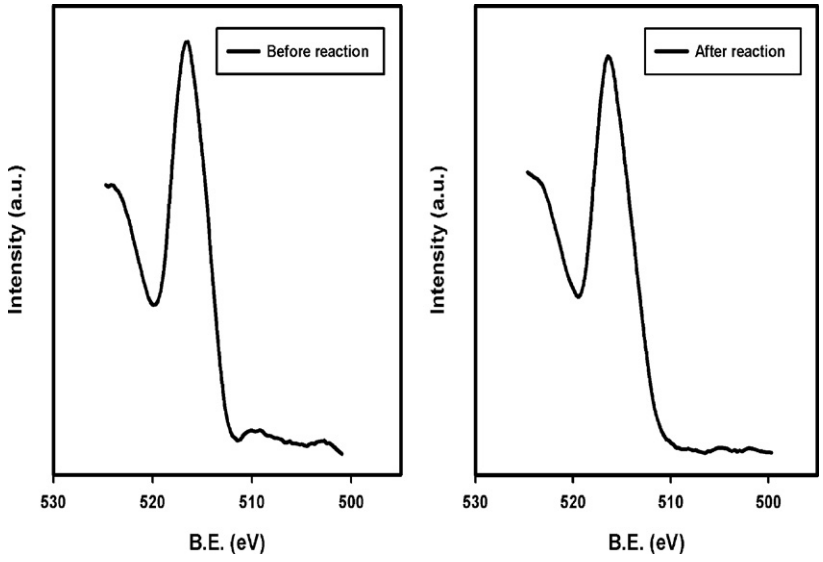

Fig. 8. XPS spectra of V $2p_{3/2}$ for the 7 wt.% V/Fe-PILC catalyst before reaction and after reaction.

The catalytic activity of the support Fe-PILC without vanadia impregnation was investigated to determine the influence of vanadia loading. Fig. 6 shows the effect of temperature on the catalytic performance of the Fe-PILC support for H_2S oxidation with a reactant composition of $H_2S/O_2/He = 5/2.5/92.5$ at GHSV = 10,000 h^{-1}. Fe-PILC showed a conversion of approximately 61% at 220 °C, which increased with temperature and reached a maximum of 79% at 300 °C. The catalytic performance of the initial clay was also examined to determine the effect of pillaring of Fe_2O_3 species into the clay layer. No H_2S conversion was observed for the initial clay at 220–300 °C.

Fig. 7 shows the time variant conversion and selectivity for SO_2 using 7 wt.% V/Fe-PILCs at 280 °C with a reactant composition of $H_2S/O_2/He = 5/2.5/92.5$ at GHSV = 10,000 h^{-1}. In the initial stage of the reaction, the H_2S conversion was 100%, and it decreased to 98.4% with time. Also, some amount of SO_2 formed in the first part of the reaction (the first 60 min). However, with more time on stream, the selectivity for SO_2 decreased with an increase in sulfur production. Similar behavior was reported by Park et al. [49] and Yasyerli et al. [50] using vanadia-based catalysts in the catalytic oxidation of H_2S.

Fig. 8 shows the XPS spectra of V $2p_{3/2}$ for the 7 wt.% V/Fe-PILC catalyst before and after the reaction. XPS spectra of the used V/Fe-PILC showed that the V $2p_{3/2}$ peaks were shifted to lower binding energy (515.6 eV) after the reaction. This indicates that fresh catalysts with vanadium in the +5 oxidation state after reduction to the +4 oxidation state increase its selectivity for elemental sulfur. This result indicates that a highly oxidized form of vanadium (V^{5+}) produced some SO_2, and a partially reduced form of vanadium containing (V^{4+}) was highly selective for the production of elemental sulfur via a redox mechanism [36,49,50].

4. Conclusions

The selective catalytic oxidation of hydrogen sulfide over V/Fe-PILC catalysts was investigated in this study. The prepared catalysts were analyzed using various physico-chemical characterization techniques. The successful pillaring of clay layers by iron species was confirmed by an increase in the d-spacing, higher surface area, increase in Fe_2O_3 content, and increases in acidity and thermal stability. V/Fe-PILC catalysts showed very good conversion of H_2S without much emission of SO_2 at 220–300 °C. A time variant study of the conversion of H_2S and selectivity for SO_2 showed that some SO_2 formed at the beginning of the reaction. XPS spectra showed that fresh catalysts with vanadium in the +5 oxidation state after the reaction were reduced to the +4 oxidation state. The catalytic performance of the initial clay was also examined to determine the influence of the pillaring of Fe_2O_3 species into the clay layer. No H_2S conversion was observed for the initial clay at 220–300 °C.

Acknowledgements

This study was supported by the National Research Foundation of Korea (2009-0070580), Brain Korea 21 program, and Korea Basic Science Institute.

References

[1] J.A. Lagas, J. Borsboom, P.H. Berben, Oil Gas J. 10 (1988) 68–71.
[2] H. Pahlavanzadeh, M. Farazar, Korean J. Chem. Eng. 26 (2009) 1112–1118.
[3] J. Wieckowska, Catal. Today 24 (1995) 405–465.
[4] A. Zey, S. White, D. Johnson, Chem. Eng. Prog. 76 (1980) 76–78.
[5] R. Kettner, N. Liermann, Oil Gas J. 11 (1982) 63–66.
[6] P.F.M.T. van Nisselrooy, J.A. Lagas, Catal. Today 16 (1993) 263–271.
[7] C.Y. Ryu, S.D. Yeo, Korean J. Chem. Eng. 27 (2010) 602–608.
[8] Y. Ahn, H. Kim, J.W. Lee, Korean J. Chem. Eng. 27 (2010) 723–728.
[9] D.E.W. Vaughan, Catal. Today 2 (1988) 187–198.
[10] A. Gil, L.M. Gandia, J.A. Vicente, Catal. Rev. Sci. Eng. 42 (2000) 145–212.
[11] J.T. Kloprogge, J. Porous Mater. 5 (1998) 5–41.
[12] J.L. Valverde, A. de Lucas, P. Sanchez, F. Dorado, A. Romero, Appl. Catal. B 43 (2003) 43–56.
[13] T.J. Pinnavaia, M.-S. Tzou, S.D. Landau, R.J. Raythatha, J. Mol. Catal. 27 (1984) 195–212.
[14] A. Corma, Chem. Rev. 97 (1997) 2373–2419.
[15] S. Yamanaka, M. Hattori, Catal. Today 2 (1988) 261–270.
[16] M.A. Martin-Luengo, H. Martins-Carvalho, J. Ladriere, P. Grange, Clay Miner. 24 (1989) 495–504.
[17] P. Yuan, H.P. He, F. Bergaya, D.Q. Wu, Q. Zhou, J. Zhu, Micropor. Mesopor. Mater. 88 (2006) 8–15.
[18] R.K. Shamsudeen, K. Nisha, S. Sugunan, React. Kinet. Catal. Lett. 81 (2004) 341–348.
[19] J.P. Chen, M.C. Hausladen, R.T. Yang, J. Catal. 151 (1995) 135–146.
[20] E.G. Rightor, M.S. Tzou, T.J. Pinnavaia, J. Catal. 130 (1991) 29–40.
[21] M.N. Timofeeva, S.Ts. Khankhasaeva, Yu.A. Chesalov, S.V. Tsybulya, V.N. Panchenko, E.Ts. Dashinamzhilova, Appl. Catal. B 88 (2009) 127–134.
[22] R. Burch, C.I. Warburton, J. Catal. 97 (1986) 503–510.
[23] B.M. Choudary, M.L. Kantam, M. Sateesh, K.K. Rao, P.L. Santhi, Appl. Catal. A 149 (1997) 257–264.
[24] P. Wu, W. Wu, S. Li, N. Xing, N. Zhu, P. Li, J. Wu, C. Yang, Z. Dang, J. Hazard. Mater. 169 (2009) 824–830.
[25] D. Nguyen-Thanh, T.J. Bandosz, J. Phys. Chem. B 107 (2003) 5812–5817.
[26] K.-T. Li, T.-Y. Chien, Catal. Lett. 57 (1999) 77–80.
[27] S. Yasyerli, G. Dogu, T. Dogu, Catal. Today 117 (2006) 271–278.
[28] E.K. Lee, K.D. Jung, O.S. Joo, Y.G. Shul, Appl. Catal. A 284 (2005) 1–4.
[29] N. Keller, C. Pham-Huu, M.J. Ledoux, Appl. Catal. A 217 (2001) 205–207.
[30] T.N. Mashapa, J.D. Rademan, M.J. Janse van Vuuren, Ind. Eng. Chem. Res. 4 (2007) 6338–6344.
[31] V.V. Shinkarev, A.M. Glushenkov, D.G. Kuvshinov, G.G. Kuvshinov, Appl. Catal. B 85 (2009) 180–191.
[32] M.D. Soriano, J. Jimenez Jimenez, P. Concepcion, A. Jimenez Lopez, E. Rodriguez Castellon, J.M. Lopez Nieto, Appl. Catal. B 92 (2009) 271–279.
[33] D. Long, Q. Chen, W. Qiao, L. Zhan, X. Liang, L. Ling, Chem. Commun. (2009) 3898–3900.
[34] K. Polychronopoulou, F. Cabello Galisteo, M. Lopez Granados, J.L.G. Fierro, T. Bakas, A.M. Efstathiou, J. Catal. 236 (2005) 205–220.
[35] D.R. Cho, S.Y. Kim, D.W. Park, P.H. Mutin, Korean J. Chem. Eng. 26 (2009) 377–381.
[36] K.V. Bineesh, D.K. Kim, D.W. Kim, H.J. Cho, D.W. Park, Energy Environ. Sci. 3 (2010) 302–310.
[37] K.V. Bineesh, S.Y. Kim, B.R. Jermy, D.W. Park, J. Mol. Catal. A 308 (2009) 150–158.
[38] F. Dorado, A. de Lucas, P.B. Garcia, A. Romero, J.L. Valverde, Appl. Catal. A 305 (2006) 189–196.
[39] B.G. Mishra, G. Ganga Rao, J. Porous Mater. 10 (2003) 93–103.
[40] K.V. Bineesh, D.R. Cho, S.Y. Kim, B.R. Jermy, D.W. Park, Catal. Commun. 9 (2008) 2040–2043.
[41] K.V. Bineesh, S.Y. Kim, B.R. Jermy, D.W. Park, J. Ind. Eng. Chem. 15 (2009) 207–211.
[42] J.L. Valverde, A. Romero, R. Romero, P.B. Garcia, M.L. Sanchez, I. Asencio, Clay Clay Miner. 53 (2005) 613–621.
[43] K.V. Bineesh, D.K. Kim, M.I. Kim, M. Selvaraj, D.W. Park, Dalton Trans. 40 (2011) 3938–3945.
[44] R.Q. Long, R.T. Yang, J. Catal. 196 (2000) 73–85.
[45] K.V. Bineesh, D.K. Kim, H.J. Cho, D.W. Park, J. Ind. Eng. Chem. 16 (2010) 593–597.
[46] N.N. Binitha, S. Sugunan, Micropor. Mesopor. Mater. 93 (2006) 82–89.
[47] K.V. Bineesh, D.K. Kim, M.I. Kim, D.W. Park, Appl. Clay Sci. (2011), doi:10.1016/j.clay.2010.12.022.
[48] J. Arfaoui, L.K. Boudali, A. Ghorbel, G. Delahay, Catal. Today 142 (2009) 234–238.
[49] D.W. Park, B.K. Park, D.K. Park, H.C. Woo, Appl. Catal. A 223 (2002) 215–224.
[50] S. Yasyerli, G. Dogu, I. Ar, T. Dogu, Chem. Eng. Sci. 59 (2004) 4001–4009.